doi.org/10.1002/batt.202000210

VIP *Very Important Paper*

Singlet Oxygen in Lithium–Oxygen Batteries

Misun Hong*[a] and Hye Ryung Byon*[b, c]

Singlet oxygen ($^1O_2$) is one of the most critical species leading to parasitic side reactions and poor reversibility in non-aqueous Li–O_2 batteries. $^1O_2$ is generated via the disproportionation of the superoxide radical ($O_2^{\bullet-}$) in O_2/Li_2O_2 electrochemistry. The mechanistic and computational studies on $^1O_2$ formation revealed the significant roles of the associated cations, solvation ability of aprotic solvents, H^+ source, and catalyst/electrode materials. Along with efforts to alleviate $^1O_2$ production, trapping and eliminating $^1O_2$ have been attempted using molecular agents. Anthracene derivatives trap $^1O_2$ and form endoperoxides, which can be quantitatively detected using *in situ* fluorescence analysis. Physical quenchers that convert $^1O_2$ to $^3O_2$ are desirable for cycling of Li–O_2 cells because quencher molecules are reusable. We highlight the recent reports on the formation and elimination of $^1O_2$, and challenges and perspectives of suppressing the $^1O_2$ effect on the performance of Li–O_2 cells.

1. Introduction

The use of Li–O_2 batteries for electric vehicles (EVs) has been intensively investigated during the last decades. Because the O_2 electrode affords the maximum specific capacity of ~700 mAh g_{total}^{-1}, which is around 2–4 times higher than the conventional intercalation electrodes, the driving range of EVs can be extended using Li–O_2 batteries.[1] These green batteries use O_2 gas from the atmosphere during discharging and reproduce it during charging. Thus, O_2 reduction and evolution reactions govern the capacity and stability of Li–O_2 cells. However, once O_2 is reduced to the superoxide radical ($O_2^{\bullet-}$), nucleophilic reactions become significant, and the non-aqueous electrolyte solution and carbonaceous electrode are destabilized.[2] Severe side reactions generate undesired products, such as lithium carbonates and carboxylates, and cause poor cyclability owing to the accumulation of side products. Therefore, many researchers have focused on analyzing the chemical reactions of $O_2^{\bullet-}$[3] and on developing catalysts for the facile decomposition of the discharging product (Li_2O_2) and side products.[4]

Conversely, it was suggested that the $O_2^{\bullet-}$ species in non-aqueous Li–O_2 cells were more stable than anticipated.[3c] Instead, the high reactivity of singlet oxygen ($^1O_2$) was proposed to ascribe detrimental reactions in Li–O_2 batteries[5] as well as in Li-ion batteries.[6] Decomposing non-aqueous electrolytes by $^1O_2$ have been highlighted through experimental and mechanistic studies.[5b,6a,7] In addition, the $^1O_2$ reacts with carbon electrode[8] and redox mediators that are used in Li–O_2 batteries to decrease charging overpotential or increased capacity.[4e,9] The $^1O_2$ as the excited form of O_2 is indicated as $^1\triangle_g$. Figure 1 shows distinct $^1O_2$ molecular orbital from the ground state of triplet O_2 indicated as $^3O_2$ or $^3\Sigma_g^-$. Recently, many researchers have investigated the quantitative detection of $^1O_2$ during discharging and charging in Li–O_2 cells, and its quenching to enhance cell stability. In this minireview, we introduce the recent progress in Li–O_2 cells, including the parameters and conditions for the formation or quenching of $^1O_2$.

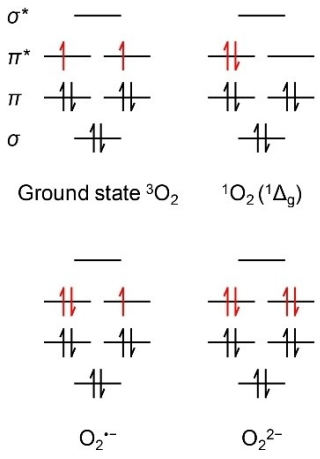

Figure 1. Molecular orbitals of O_2 in the ground state ($^3\Sigma_g^-$) and the first excited state ($^1\Delta_g$) and in the reduced forms of superoxide ($O_2^{\bullet-}$) and peroxide (O_2^{2-}).

[a] *Dr. M. Hong*
Surface and Interface Science Laboratory
RIKEN
2-1 Hirosawa, Wako, Saitama 351-0198, Japan
E-mail: misun.hong@riken.jp
[b] *Prof. H. R. Byon*
Department of Chemistry
Korea Advanced Institute of Science and Technology (KAIST)
291 Daehak-ro, Yuseong-gu, Daejeon 34141, Republic of Korea
[c] *Prof. H. R. Byon*
Advanced Battery Center
KAIST Institute for NanoCentury
291 Daehak-ro, Yuseong-gu, Daejeon 34141,
Republic of Korea
E-mail: hrbyon@kaist.ac.kr

Supporting information for this article is available on the WWW under https://doi.org/10.1002/batt.202000210

2. $^1O_2$ Formation via Superoxide Disproportionation

Non-aqueous Li–O_2 cells are discharged via the O_2 reduction reaction, which forms lithium peroxide (Li_2O_2), and charged via the decomposition of Li_2O_2. The overall charge–discharge reaction can be expressed as follows [Eq. (1)]:

$$2Li_{(s)} + O_{2(g)} \rightleftharpoons Li_2O_{2(s)}, \qquad E = 2.96\,V \text{ vs. } Li/Li^+ \tag{1}$$

The intermediate $O_2^{\bullet-}$ is initially formed by the first electron-transfer during discharge [Eq. (2)]. If $O_2^{\bullet-}$ is preferentially adsorbed on the electrode surface, successive electron transfer produces Li_2O_2 [Eq. (3), where the asterisk symbol indicates the surface adsorption). Alternatively, $O_2^{\bullet-}$ undergoes disproportionation and yields $^1O_2/^3O_2$ along with Li_2O_2 [Eq. (4)], which occurs for both solvated and surface-adsorbed states of $O_2^{\bullet-}$.[2a,10]

$$O_{2(g)} + e^- \rightarrow O_2^{\bullet-} \tag{2}$$

$$O_2^{\bullet-*} + e^- + 2Li^+ \rightarrow Li_2O_{2(s)} \tag{3}$$

$$2O_2^{\bullet-} + 2Li^+ \rightarrow Li_2O_{2(s)} + {}^3O_2/{}^1O_2 \tag{4}$$

During charging, Li^+ is dissolved from the Li_2O_2 surface [Eq. (5)]. The remaining Li-deficient phase (*i.e.*, $Li_{2-x}O_2$) is decomposed and generates $^1O_2$ or $^3O_2$ [Eq. (6–1)], or releases $O_2^{\bullet-}$ [Eq. (6–2)].[11] These different charging processes in Eqs. (6–1) and (6–2) are determined by the $O_2^{\bullet-}$ solvation ability of the non-aqueous electrolyte.

$$Li_2O_{2(s)} \rightarrow Li_{2-x}O_{2(s)} + x(Li^+ + e^-) \tag{5}$$

$$Li_{2-x}O_{2(s)} \rightarrow {}^3O_2/{}^1O_2 + (2-x)\ (Li^+ + e^-) \tag{6-1}$$

$$Li_{2-x}O_{2(s)} \rightarrow O_2^{\bullet-}{}_{(sol)} + (2-x)\ Li^+ + (1-x)\ e^- \tag{6-2}$$

The $^1O_2/^3O_2$ evolution during charge in Eq. (6–1) is also applied for Li_2O_2.[1c] Beyond Eqs. (5)–(6), there are several ways to evolve $^1O_2$ during charge. The disproportionation of $O_2^{\bullet-}$ in Eq. (4) can be undertaken during charging processes. Direct electrochemical oxidation of $O_2^{\bullet-}$ is also thermodynamically possible to generate $^1O_2$.[5b,12] In addition, the oxidative decomposition of side product Li_2CO_3 can generate $^1O_2$.[13] All these processes contribute to enlarged $^1O_2$ yield during the charging process.

2.1. Effect of Cations on $^1O_2$ Formation

Mourad *et al.*[14] revealed that the ion association between the $O_2^{\bullet-}$ and cation (M^+) in the electrolyte solution significantly influences the $O_2^{\bullet-}$ disproportionation process (Figure 2a). The larger alkali ion K^+ sufficiently stabilizes $O_2^{\bullet-}$ and leads to negligible disproportionation of $O_2^{\bullet-}$ to form $^1O_2$,[15] whereas the $^1O_2$ yield is largely dependent on the $O_2^{\bullet-}$ association with Li^+ and Na^+. The $O_2^{\bullet-}$ associated with both Li^+ and Na^+ forms dimers or clusters ($(MO_2)_n$, where n is an integer),[16] and the energy barriers for these products influence the yield of $^1O_2$ [Eq. (7), Figure 2b].[14]

$$2MO_2 \rightarrow ({}^3M(O_2)_2M) \text{ or } ({}^1M(O_2)_2M) \rightarrow M_2O_{2(s)} + {}^3O_2/{}^1O_2 \tag{7}$$

Accordingly, the yields of $^1O_2$ were different; Na^+ led to a higher $^1O_2$ yield than Li^+. Density functional theory (DFT) calculations elucidated that a singlet dimer containing Na^+ ($^1Na(O_2)_2Na$) had low reaction barrier than a triplet one during the first step of Eq. (7), whereas Li^+ is thermodynamically favorable to make a triplet dimer ($^3Li(O_2)_2Li$). When Li^+ was mixed with tetrabutylammonium (TBA^+), a singlet dimer could be formed ($^1Li(O_2)_2Li$, red line, Figure 2b) via an intermediate $Li(O_2)_2^-\cdots(TBA^+)$ species (black line, Figure 2b). Increasing $^1O_2$ yield resulted in undesired reactions and the accumulation of carbonaceous side products.

If trace water is present in Li–O_2 and Na–O_2 cells, the solubility of $O_2^{\bullet-}$ is increased. It may enhance yields of both $^1O_2$ and $^3O_2$. However, the effect of water has been controversial for a long time. Numerous previous studies found $^1O_2$ by adding water as the H^+ source.[12,17] H^+ combines with $O_2^{\bullet-}$ to form $HOO^\bullet$ species [Eq. (8)]. The $HOO^\bullet$ is the key intermediate and leads to H^+-mediated $O_2^{\bullet-}$ disproportionation; Eq. (9) shows that $HOO^\bullet$ is involved in the production of $^1O_2$ via either the nucleophilic attack of $O_2^{\bullet-}$ [Eq. (9–1)] or chemical reaction with water [Eq. (9–2)].[17–18] On the contrary, there are also several

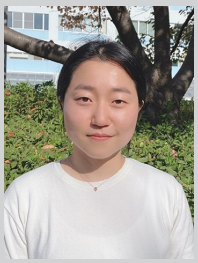

Dr. Misun Hong received her Ph. D. in Chemistry from Pohang University of Science and Technology in 2015. She worked as a postdoctoral researcher at RIKEN, Korea Advanced Institute of Science and Technology, and Institute for Basic Science (2015–2018). She is currently a postdoctoral researcher at RIKEN. Her research interests are interfacial phenomena and low-dimensional materials in electrochemical application systems.

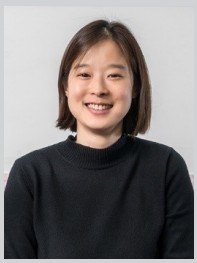

Dr. Hye Ryung Byon received Ph. D degree (2008) from Materials and Inorganic chemistry at POSTECH (Pohang University of Science and Technology) in South Korea. After a postdoctoral period at MIT (2008~2010), she started her career as a principal investigator at Byon Initiative Research Unit, RIKEN in Japan. In 2016, she moved to KAIST (Korea Advanced Institute of Science and Technology), department of chemistry in South Korea. Currently, she is an associate professor and also an adjunct professor at Advanced Battery Center, KAIST Institute for NanoCentury.

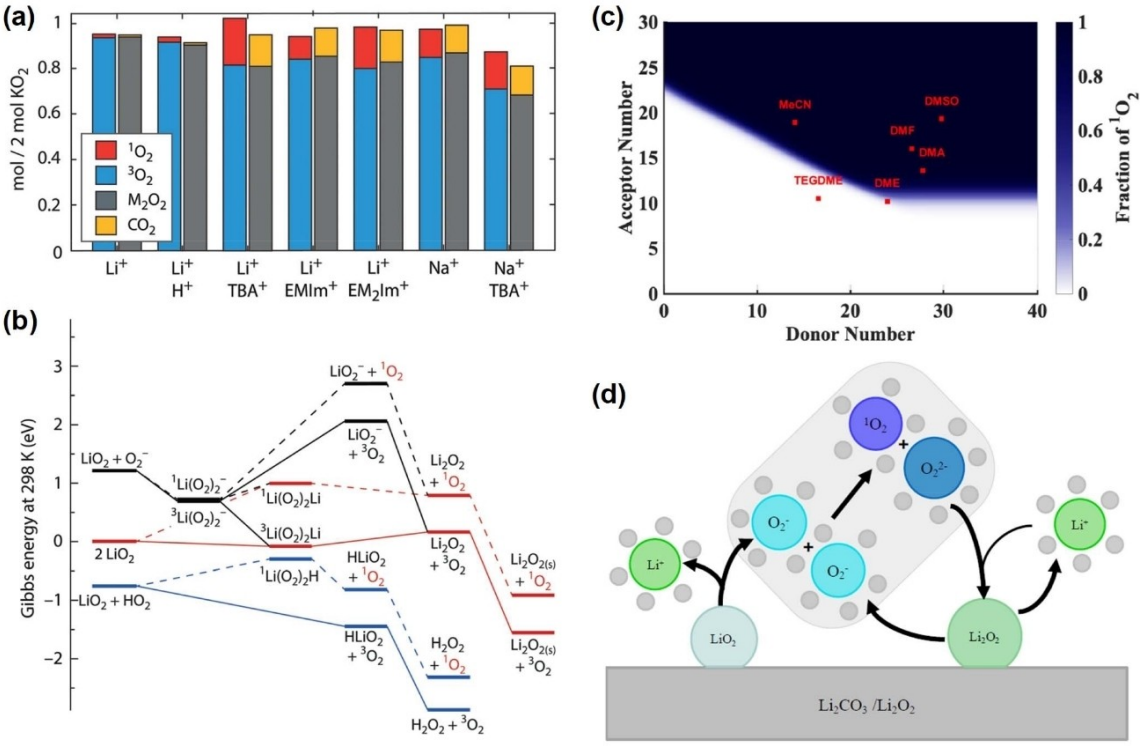

Figure 2. $^1O_2$ generation relying on a–b) the cations and c–d) aprotic solvents. a) Amounts of $^3O_2$, $^1O_2$, Li_2O_2 (or Na_2O_2), and CO_2 yielded from different electrolytes, containing 0.5 M Li^+ or Na^+, KO_2, and 18-crown-6 in TEGDME. Additives were either CF_3COOH as a H^+ source, or 0.1 M large-size cations of TBA^+, $EMIm^+$ (3-ethyl-1-methyl-1*H*-imidazol-3-ium), and EM_2Im^+ (3-ethyl-1,2-dimethyl-1*H*-imidazol-3-ium). b) Gibbs free energy diagrams of $O_2^{\bullet-}$ disproportionation processes in the electrolytes of Li^+ alone (red), $Li^+ + TBA^+$ (black), and $Li^+ + H^+$ (blue). c) $^1O_2$ fractions correlated with acceptor number and donor number of aprotic solvents. d) Schematic illustration of $O_2^{\bullet-}$ and Li^+ dissolution and subsequent $O_2^{\bullet-}$ disproportionation during charging. (a–b) Reproduced from Ref. [14] with permission. Copyright 2019 The Royal Society of Chemistry. (c–d) Reproduced from Ref. [13b] with permission. Copyright 2020 American Chemical Society.

reports that H^+ unlikely aids in forming $^1O_2$.[19] Similar debates are also found in Li–O_2 cells. Mahne *et al.*[5b] reported that the amounts of $^1O_2$ generated in the absence and presence of 1,000 ppm of water were ~4% and ~6% of the theoretical amount, respectively. Increasing $^1O_2$ yield with H_2O suggests that water promotes the H^+-mediated $O_2^{\bullet-}$ disproportionation. Pierini *et al.*[20] supported a similar result forming $^1O_2$ using H^+ through computational simulation, while predicting the energetic unfeasibility for the $^1O_2$ formation in the absence of H^+. Detecting ~4% $^1O_2$ in the absence of water injection is understood by a trace amount of water that is always included in the cells. This H^+-mediated $O_2^{\bullet-}$ disproportionation is particularly significant in Na–O_2 cells, where $HOO^\bullet$ leads to form both NaO_2 and $^1O_2$.[21]

$$O_2^{\bullet-} + H^+ \rightarrow HOO^\bullet \quad (8)$$

$$HOO^\bullet + O_2^{\bullet-} \rightarrow HO_4^- \rightarrow HOO^- + {}^3O_2/{}^1O_2 \quad (9\text{-}1)$$

$$2HOO^\bullet + H_2O \rightarrow H_2O_4 + H_2O \rightarrow H_2O_2 + H_2O + {}^3O_2/{}^1O_2 \quad (9\text{-}2)$$

In contrast, Mourad *et al.*[14] reported that H^+ presented a negligible effect on the production of $^1O_2$ in the Li–O_2 cells. They used trifluoroacetic acid (CF_3COOH) as the H^+ source instead of water, and incorporated KO_2 as an $O_2^{\bullet-}$ source in lithium bis(trifluoromethanesulfonyl)imide (LiTFSI)/tetraethylene glycol dimethyl ether (TEGDME) electrolyte solution. The result showed a marginal change of $^1O_2$ yield (the second set of bar graphs labeled "Li^+ H^+" in Figure 2a). DFT calculations supported the preferential production of $^3O_2$ in this condition (blue lines, Figure 2b). We should note that a distinct result was found in Na–O_2 cells. Lozano *et al.*[21b] reported that the addition of Brønsted-Lowry acid NH_4^+ generated $^1O_2$ through the H^+-mediated $O_2^{\bullet-}$ disproportionation, which provided larger $^1O_2$ amount compared to the absence of the H^+ source. The role of H_2O and H^+ related to the $^1O_2$ formation is still complicated and inconclusive. Because water can alter not only the main intermediates but also the degree of $O_2^{\bullet-}$ solvation that determines Li–O_2 and Na–O_2 reaction pathways,[10b] further systematic investigations should be needed in the future.

2.2. Effect of $O_2^{\bullet-}$ Solvation on $^1O_2$ Formation

Houchins *et al.*[13b] focused on the disproportonation of solvated $O_2^{\bullet-}$ for $^1O_2$ formation. As aforementioned, Li^+ stabilizes $O_2^{\bullet-}$ by forming LiO_2 and lowers the possible formation of $^1O_2$. On the contrary, the free $O_2^{\bullet-}$ allows $^1O_2$ formation [Eq. (10)].

$$2O_2^{\bullet-}{}_{(sol)} \rightarrow O_2^{2-}{}_{(sol)} + {}^3O_2/{}^1O_2 \quad (10)$$

It is predicted that Gutmann acceptor and donor numbers (AN and DN, respectively) significantly determine the solvation ability of aprotic solvents rather than their dielectric constants. The solvents with high AN or high DN lead to high concentrations of $O_2^{\bullet-}$ and $^1O_2$. TEGDME and dimethoxyethane (DME) have moderate AN and DN and suppress the $^1O_2$ production as shown in Figure 2c.

The solvation effect was also applied to the charging process (Figure 2d). For example, solvents with high DN and AN preferentially dissolved the Li^+ ions and $O_2^{\bullet-}$ species, respectively, from the $Li_{2-x}O_2$ or Li_2O_2 [Eq. (6–2)]. Wang *et al.*[11c] showed that the higher DN solvent DMSO aided in forming $O_2^{\bullet-}$ more than diethylene glycol dimethyl ether (DEGDME). Subsequent dissolution of $O_2^{\bullet-}$ species and the disproportionation of $O_2^{\bullet-}$ produced $^1O_2$ [Eq. (10)]. It therefore underscores that the solvation power leading to the dissolution of $O_2^{\bullet-}$ is not beneficial for both the discharging and charging process in Li–O_2 cells.

2.3. Effect of Electrode Material on $^1O_2$ Formation

Various electrocatalysts were developed for the facile oxidation of Li_2O_2 and the side products during charge.[4a,d] Samojlov *et al.*[22] evaluated the effects of catalysts for the production of $^1O_2$. They utilized carbon-free TiC nanoparticles; catalyst-carbon hybrid materials incorporating α-MnO_2 nanorods, Co_3O_4 nanorods, and Pd nanoparticles; and carbon-based materials, such as Super P (SP) carbon particles and hydrophilic SP (SP hp) (Figure 3a). The $^1O_2/2e^-$ yield was estimated by adding the $^1O_2$ trapping agent 9,10-dimethylanthracene (DMA) (Figures 3b–c). The α-MnO_2, Co_3O_4, and Pd catalysts produced 1–2% $^1O_2$ during charge with 0.1 M $LiClO_4$/TEGDME. By comparison, TiC, SP hp, and SP exhibited 6%, 4%, and 3% of the $^1O_2$ yield, respectively. It reveals lower $^1O_2$ formation using the catalysts compared to that using carbon electrodes, and the analogous tendency was also obtained during discharge. However, the highest $^1O_2$ yield from the carbon-free TiC is anomalous. They envisioned the disproportionation of hydrogen peroxide (H_2O_2) on the TiC. H_2O_2 could be generated from the impurity of H_2O and H^+ sources, and TiC catalyzed the reaction to produce $^1O_2$ [Eq. (11)]. By detecting considerable $^1O_2$ evolution when H_2O_2 was added to the TiC electrode, they could support this hypothesis.

$$2H_2O_2 \xrightarrow{cat.} 2H_2O + {}^3O_2/{}^1O_2 \quad (11)$$

3. Detection of $^1O_2$ in Li–O_2 Cells

$^1O_2$ was firstly detected in Li–O_2 cells using the electron paramagnetic resonance (EPR) technique. Wandt *et al.*[5a] employed a piperidine derivative and reported the notable formation of $^1O_2$ at >3.55 V using *in situ* EPR. 2,2,6,6-tetramethyl-4-piperidone (4-oxo-TEMP, **1**, Figure 4a) reacted with $^1O_2$, it formed 4-oxo-2,2,6,6-tetramethyl-1-piperidinyloxy (4-oxo-TEMPO, Figure 4b).[23] The amount of trapped $^1O_2$ was estimated to ~0.5% of the total O_2 amount in the potential range of 3.55–3.75 V (Figure 5a).

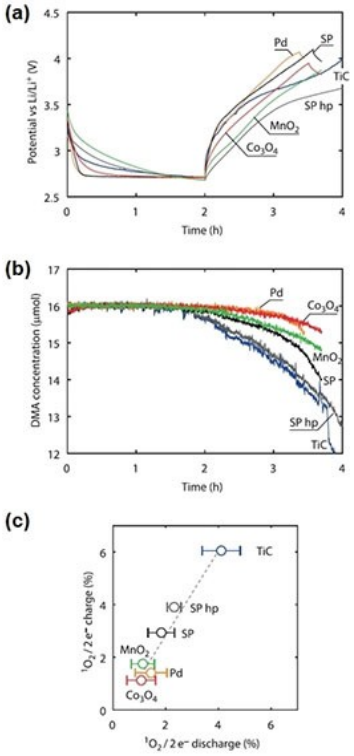

Figure 3. Correlation between catalyst/electrode materials and $^1O_2$ formation. SP is Super P carbon, and SP hp is hydrophilic SP. Pd, Co_3O_4, and α-MnO_2, particles were deposited on carbon. a) Potential profiles for discharge and charge with 0.1 M $LiClO_4$/TEGDME + 16 μM DMA, and b) corresponding *in situ* fluorescence decay. c) The $^1O_2$ yields measured for charge and discharge. *Ex situ* HPLC with 30 mM DMA was used to detect $^1O_2$ during discharge. Reproduced from Ref. [22] with permission. Copyright 2020 Elsevier.

More general methods are photo-detections. The emission of $^1O_2$ was directly detected at a wavelength of 1270 nm.[5b,17a] After the disproportionation of $O_2^{\bullet-}$, the resulting $^1O_2$ was transitioned to $^3O_2$ in evolving this spin-forbidden emission. In comparison, the collision of two $^1O_2$ molecules follows the spin-allowed transition with emission at 633 nm.[6b] Nonetheless, both emission signals are extremely weak, and the $^1O_2$ lifetime is also very short. Alternatively, $^1O_2$ can be sensitively detected using trapping agents that form $^1O_2$-complex. The trapping agents are chemically and irreversibly transformed after reacting with $^1O_2$. Representatives are **1**–**3** in Figure 4a, and the chemical reactions with $^1O_2$ are depicted in Figure 4b–c. These trapping agents have intense spectral signal and a long lifetime to quantitatively analyze chemical quenching by $^1O_2$-complex. For example, the absorption/emission spectra of DMA appear 300–700 nm region, and their signals are reduced after capturing $^1O_2$ via [4 + 2] cycloaddition (Figure 4c).[5b] Various examples of adapting trapping agents to Li–O_2 and Na–O_2 cells are summarized in Table S1[5,13a,14,21,22,24,26,31] in the Supporting Information. Delithiated lithium iron phosphate ($Li_{1-x}FePO_4$)

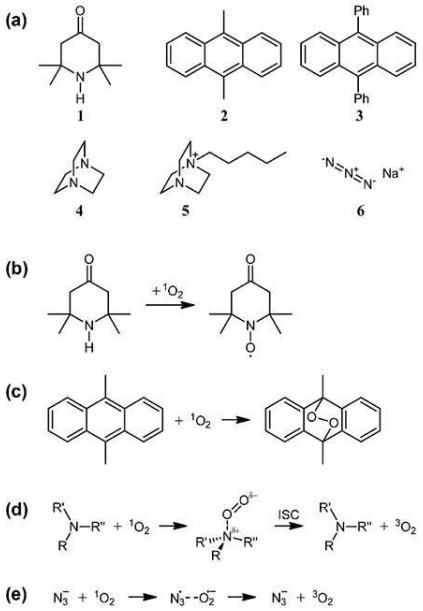

Figure 4. Trapping and quenching agents of $^1O_2$ used for Li–O_2 cells. a) **1**: 2,2,6,6-tetramethyl-4-piperidone (4-oxo-TEMP), **2**: 9,10-dimethylanthracene (DMA), **3**: 9,10-diphenylanthracene (DPA), **4**: diazabicyclo[2.2.2]octane (DABCO), **5**: 1-pentyl-1,4-diazabicyclo[2.2.2]octan-1-ium (DABCOnium), and **6**: sodium azide (NaN_3). b–c) Chemical reactions between the agents and $^1O_2$; b) nitroxide radicals for piperidine (**1**), and c) endoperoxides for anthracene (**2**, **3**). d–e) Physical quenching of $^1O_2$ using d) amines (**4**, **5**) and e) azides (**6**). ISC is intersystem crossing.

was used as the anode to avoid unintended decomposition of the trapping agents.

Mahne *et al.*[5b] used 9,10-dimethylanthracene (DMA, **2**) and 9,10-diphenylanthracene (DPA, **3**) to trap $^1O_2$. These fluorescent anthracene derivatives are converted into non-fluorescent endoperoxides via [4 + 2] cycloaddition (Figure 4c). DMA can trap $^1O_2$ twice as fast as DPA; therefore, DMA was used in many studies. *In situ* fluorescence measurements revealed that a loss of fluorescence of DMA by trapping $^1O_2$ occurred from the beginning stage of the charging process at ~3 V (Figure 5b). The quantity of $^1O_2$ was measured to be ~4% of the total charge during charge. *Ex situ* high-performance liquid chromatography (HPLC) technique was also used to detect sparse $^1O_2$ after discharge.

DMA-containing Li–O_2 cells exhibited e^-/O_2 values closer to 2 during for both discharge and charge by eliminating $^1O_2$ compared to the cells without DMA (solid lines, Figure 5d). In addition, the amount of carbonaceous side products was reduced by approximately 70% for discharge in the presence of 30 mM DMA (Figure 6a–b, 800 mAh g^{-1}). During charge, the CO_2 evolution was diminished by 30-fold (dashed lines, Figure 5d), which confirmed the removal of $^1O_2$ in Li–O_2 cells. However, anthracene derivatives present poor solubility and are disposable after they are converted into endoperoxides. For example, 30 mM DMA was entirely used during discharge at a capacity of 800 mAh g^{-1}. It turns out that the capacity should be sufficiently small (~200 mAh g^{-1}) if 30 mM DMA was used for both discharge and charge. Therefore, the trapping agents with high solubility are needed to achieve practical $^1O_2$ indicators in Li–O_2 cells, which would demand molecular engineering by introducing substituents such as alkyl, ether groups,[24] and ionic liquid moieties.[25]

4. Removal of $^1O_2$ in Li–O_2 Cells

The detrimental $^1O_2$ should be eliminated before provoking side reactions in Li–O_2 cells. The more advanced concept is to

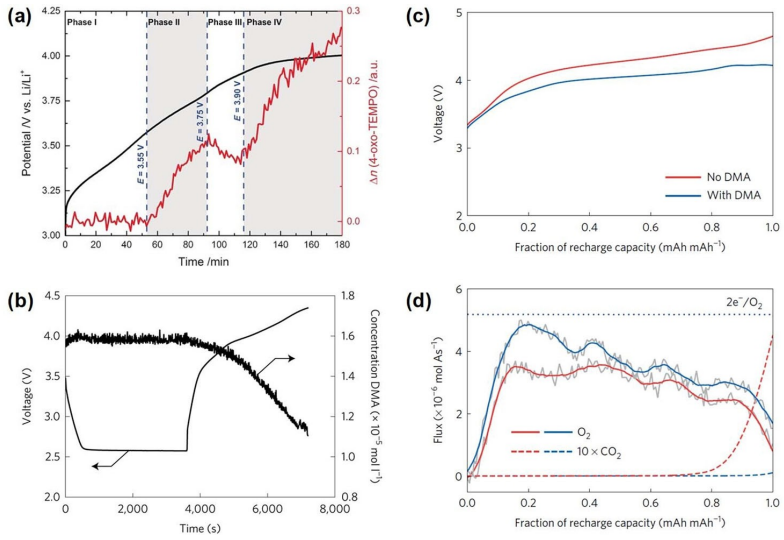

Figure 5. *In situ* $^1O_2$ detection in the Li–O_2 cells using $^1O_2$ trapping molecules and the effects of $^1O_2$ removal. a) $^1O_2$ detected by 0.1 M 4-oxo-TEMP with 0.5 M LiTFSI/DEGDME during charge. b) Galvanostatic discharging and charging profiles with 16 μM DMA in 0.1 M $LiClO_4$/TEGDME and corresponding *in situ* fluorescence measurements. c) Galvanostatic charging profiles with and without 30 mM DMA in 0.1 M $LiClO_4$/TEGDME after discharge by 200 mAh g^{-1}, and d) corresponding O_2 and CO_2 evolution profiles through gas analysis. (a) Reproduced from Ref. [5a] with permission. Copyright 2016 Wiley-VCH Verlag GmbH & Co. KGaA, Weinheim. (b–d) Reproduced from Ref. [5b] with permission. Copyright 2017 Springer Nature.

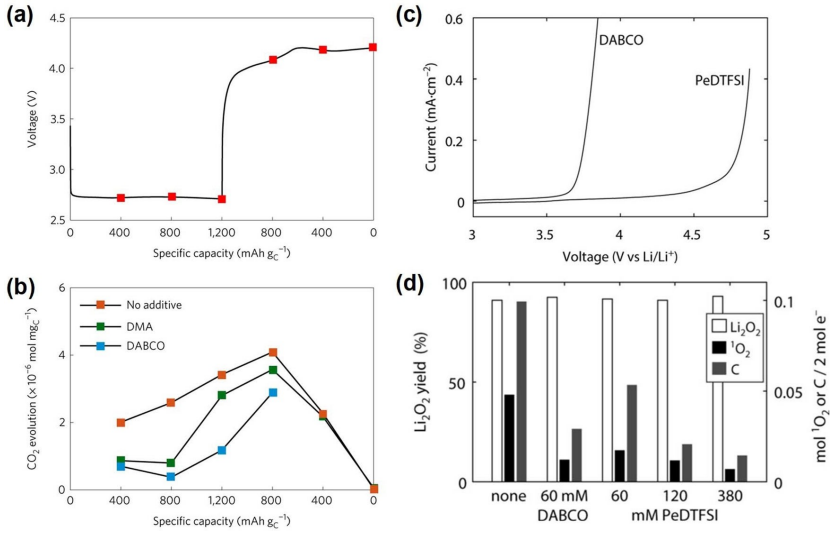

Figure 6. Effects of physical $^1O_2$ quenchers. a) Galvanostatic discharging and charging profile at a current rate of 70 mA g^{-1} with 0.1 M $LiClO_4$/TEGDME. b) Quantity of CO_2 evolution arising from the decomposed Li_2CO_3 at different stages of discharge and charge in (a). Red, green, and blue data points indicate 0.1 M $LiClO_4$/TEGDME containing no additive, 30 mM DMA and 10 mM DABCO, respectively. c) Anodic current profiles for DABCO and PeDTFSI (pentyl DABCOnium bearing TFSI anion) with 0.1 M LiTFSI/TEGDME. The scan rate was 50 mV s^{-1}. d) Quantitative analysis of Li_2O_2, $^1O_2$, and side products (indicated as C) after discharge with no additive, 60 mM DABCO and 60, 120, and 380 mM PeDTFSI. The discharging test was carried out by 1000 mAh g^{-1} and at a current rate of 100 mA g^{-1} with 1 M LiTFSI/TEGDME. (a–b) Reproduced from Ref. [5b] with permission. Copyright 2017 Springer Nature. (c–d) Reproduced from Ref. [24] with permission. Copyright 2019 Wiley-VCH Verlag GmbH & Co. KGaA, Weinheim.

convert $^1O_2$ to stable $^3O_2$ through physical quenching. The quenching agents serve as a physical quencher of $^1O_2$, and the widely-used ones are **4**–**6** in Figure 4a. Because the quenching agents regain their original forms after releasing $^3O_2$, they are re-useable as shown in Figure 4d–e.

Amine and azide derivatives, such as diazabicyclo[2.2.2]octane (DABCO, **4**, Figure 4a),[5b,13a] 1-pentyl-1,4-diazabicyclo[2.2.2]octan-1-ium (DABCOnium, **5**, Figure 4a),[24] and sodium azide (NaN_3, **6**, Figure 4a),[26] are representative physical quenchers used for Li–O_2 cells. Eq. (12) and Figure 4d–e exhibit detailed mechanism.[27]

$$Q + {}^1O_2 \underset{k_{-diff}}{\overset{k_{diff}}{\rightleftharpoons}} {}^1(Q\,{}^1O_2) \underset{k_{-ex}}{\overset{k_{ex}}{\rightleftharpoons}} {}^1(Q\,{}^1O_2)_{CT} \xrightarrow{k_p} {}^3(Q\,{}^3O_2)_{CT} \rightarrow Q + {}^3O_2 \quad (12)$$

When a quencher (Q) encounters $^1O_2$, a singlet complex (^{1}(Q $^1O_2$)) is formed. Charge transfer (CT) from Q to $^1O_2$ forms a singlet exciplex (^{1}(Q $^1O_2)_{CT}$), and the intersystem crossing (ISC) generates a triplet complex (^{3}(Q $^3O_2)_{CT}$). Thereafter, $^3O_2$ is separated from Q.

Mahne *et al.*[5b] reported that the amount of side products generated during discharge decreased by approximately 73% when 10 mM DABCO was added to $LiClO_4$/TEGDME (Figure 6a–b). Moreover, when the azide anion (N_3^-)[28] was added to LiTFSI/DMSO, $^1O_2$ was efficiently quenched during discharge.[26] However, the N_3^- ions also easily react with hydroxyl radicals ($OH^•$) and form azide radicals ($N_3^•$) and OH^- ions,[29] which decreases the quenching efficiency.

$^1O_2$ quenchers with low ionization energy expedite CT with $^1O_2$ [Eq. (12)].[27a,30] However, the low oxidation stability obstructs their utilization. For example, DABCO is oxidized at ~3.6 V[5b] and unstable in Li–O_2 cells where charging potential exceeds 4.2 V. Petit *et al.*[24] designed DABCOnium, which was highly soluble, stable at a potential of ~4.2 V, and compatible with a metallic Li electrode (Figure 6c). When 380 mM DABCOnium was added to Li–O_2 cells, the amount of side products decreased by 86% during discharge (Figure 6d). Furthermore, 2e$^-$/O_2 process was achieved up to ~4.2 V for the charge. Although the molar quenching efficiency of DABCOnium is approximately half that of DABCO (see the $^1O_2$ fractions and amounts of side products obtained using 60 mM DABCO vs. 60 mM DABCOnium, Figure 6d), the high solubility of DABCOnium can compensate for the low efficiency (380 mM DABCOnium, Figure 6d).

As another approach, redox mediators (RMs) were used as molecular catalysts to reduce the charging potential. During charge, RMs are electrochemically oxidized, and the oxidized RMs chemically decompose Li_2O_2.[4b,c] Accordingly, the charging potential of Li–O_2 cells is determined by the oxidation potential of the RMs. Kwak *et al.*[31] used 5,10-dihydro-5,10-dimethylphenazine (DMPZ) as RM to maintain the potential at ~3.2 V, and evaluated the effect of DABCO (Figure 7). The charging potential was constant over multiple cycles, where DABCO could be stable (blue profile, Figure 7b). In contrast, when DABCO alone was added to Li–O_2 cells, without DMPZ, the charging potentials significantly increased during cycles (red profile, Figure 7b). On-line electrochemical mass spectrometry (OEMS) revealed a larger amount of O_2 from the combination of DMPZ and DABCO than the one from DMPZ alone for the first charge (Figure 7c). It indicates that DABCO also stabilized DMPZ by elimination of $^1O_2$ and resulted in the improved stability of the Li–O_2 cell.[5b] This synergetic effect also caused decreased side products.[4e,9]

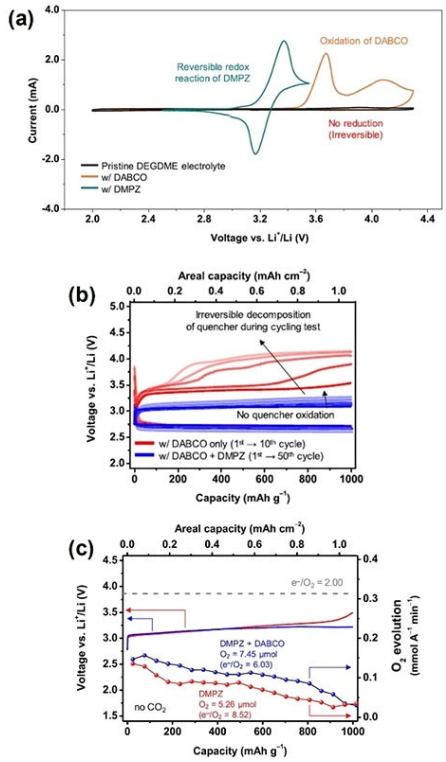

Figure 7. Effect of a redox mediator (RM), 5,10-dihydro-5,10-dimethylphenazine (DMPZ), along with DABCO. a) Cyclic voltammograms of blank (black), DMPZ (green), and DABCO (orange) in 1 M LiTFSI/DEGDME. The scan rate was 1 mV s^{-1}. b) Cycling galvanostatic profiles with 0.1 M DABCO (red) and 0.1 M DABCO + 0.2 M DMPZ (blue) at 100 mA g^{-1} in 1 M LiTFSI/DEGDME. c) Charging profile and corresponding quantitative O_2 detection with 1 M LiTFSI/TEGDME. Reproduced from Ref. [31] with permission. Copyright 2019 American Chemical Society.

In addition to the primary role of lowering charging potentials, some RMs could also act as $^1O_2$ quenchers. Liang *et al.* reported that 2,2,6,6-tetramethyl-1-piperidinyloxy (TEMPO) presented dual role as $^1O_2$ quencher and charging catalyst.[32] The oxidized TEMPO in LiTFSI/DEGDME promoted the intersystem crossing of $^1O_2$ and generated $^3O_2$, while the charging potential held ~3.7 V. All these results showed simple and optimal ways for utilizing $^1O_2$ quenchers for Li–O_2 cells in practice.

5. Summary and Outlook

We highlighted the recent essential studies on the effects of cations, $O_2^{\bullet-}$ solvation, and electrode materials on $^1O_2$ formation in Li–O_2 cells. The $O_2^{\bullet-}$ disproportionation and $^1O_2$ yield depended on the ion-pairing, solvation ability of $O_2^{\bullet-}$, and electrode materials. Comparative studies indicated that the use of soft Lewis acid, aprotic solvents with either high donor number or acceptor number, and *d*-block early transition metal species with d^0 configuration (*e.g.*, TiC) should be avoided in Li–O_2 cells because they enhanced $^1O_2$ generation. $^1O_2$ could be captured or quenched using molecular agents. The $^1O_2$ trapping molecules were used to detect the $^1O_2$ yield during the discharging and charging process and address the origin of $^1O_2$ generation in Li–O_2 cells. *In situ* fluorescence analysis revealed a small amount of $^1O_2$ generated during the first cycle (only 2–6% of the theoretical amount, as calculated using the total charges), yet its effect was significant. If $^1O_2$ generation was suppressed, the yield of side products was considerably decreased, and the number of electrons (e^-/O_2) was close to the ideal 2. The shortcomings of $^1O_2$ trapping molecules were low solubility and poor detection resolution using the fluorescence technique. Alternatively, physical quenchers transform $^1O_2$ to stable $^3O_2$, thus being practically utilized to suppress side reactions in Li–O_2 cells. The electrochemical instability of $^1O_2$ quenchers at high potentials could be resolved by the co-addition of charging catalysts, which improved cyclability of Li–O_2 cells. Based on these fundamental studies, future works will focus on restraining $^1O_2$ formation. Electrolyte solution should be carefully selected, and water content should be controlled to avoid the solution-mediated reaction that releases $O_2^{\bullet-}$. Stable quenchers should be developed further through various molecular designs. Additives enhancing molecular/ionic association of $O_2^{\bullet-}$ or redox mediators promoting two electron-transfer will also alleviate side reactions arising from $^1O_2$. Lastly, the advanced separator will be utilized to prevent $O_2^{\bullet-}$ shuttling that is produced at the Li anode.

Acknowledgments

This work was supported by National Research Foundation (NRF) of Korea Grant, funded by the Korean Government (Grant No. 2019R1A2C2007551).

Conflict of Interest

The authors declare no conflict of interest.

Keywords: energy storage · lithium–oxygen battery · singlet oxygen · singlet oxygen quenchers · superoxide disproportionation

[1] a) R. A. Wong, H. R. Byon, M. L. Thomas, K. Dokko, M. Watanabe, *Encyclopedia of Inorganic and Bioinorganic Chemistry*, **2019**, pp. 1–23; b) W. J. Kwak, Rosy, D. Sharon, C. Xia, H. Kim, L. R. Johnson, P. G. Bruce, L. F. Nazar, Y. K. Sun, A. A. Frimer, M. Noked, S. A. Freunberger, D. Aurbach, *Chem. Rev.* **2020**, *120*, 6626–6683; c) N. Mahne, O. Fontaine, M. O. Thotiyl, M. Wilkening, S. A. Freunberger, *Chem. Sci.* **2017**, *8*, 6716–6729.

[2] a) D. Aurbach, B. D. McCloskey, L. F. Nazar, P. G. Bruce, *Nat. Energy* **2016**, *1*, 16128; b) X. Yao, Q. Dong, Q. Cheng, D. Wang, *Angew. Chem. Int. Ed.* **2016**, *55*, 11344–11353; *Angew. Chem.* **2016**, *128*, 11514–11524; c) A. Khetan, H. Pitsch, V. Viswanathan, *J. Phys. Chem. Lett.* **2014**, *5*, 2419–2424; d) V. K. C. Chau, Z. Chen, H. Hu, K.-Y. Chan, *J. Electrochem. Soc.* **2016**, *164*, A284-A289; e) B. D. McCloskey, D. S. Bethune, R. M. Shelby, T. Mori, R. Scheffler, A. Speidel, M. Sherwood, A. C. Luntz, *J. Phys. Chem. Lett.* **2012**, *3*, 3043–3047; f) B. D. McCloskey, A. Speidel, R. Scheffler, D. C. Miller, V. Viswanathan, J. S. Hummelshøj, J. K. Nørskov, A. C. Luntz, *J. Phys. Chem. Lett.* **2012**, *3*, 997–1001; g) M. M. Ottakam Thotiyl, S. A. Freunberger, Z. Peng, P. G. Bruce, *J. Am. Chem. Soc.* **2013**, *135*, 494–500.

[3] a) R. Black, S. H. Oh, J.-H. Lee, T. Yim, B. Adams, L. F. Nazar, *J. Am. Chem. Soc.* **2012**, *134*, 2902–2905; b) X. Zhang, L. Guo, L. Gan, Y. Zhang, J. Wang, L. R. Johnson, P. G. Bruce, Z. Peng, *J. Phys. Chem. Lett.* **2017**, *8*, 2334–2338; c) W.-J. Kwak, J.-B. Park, H.-G. Jung, Y.-K. Sun, *ACS Energy Lett.* **2017**, *2*, 2756–2760.
[4] a) Z. Chang, J. Xu, X. Zhang, *Adv. Energy Mater.* **2017**, *7*, 1700875; b) Y. Ko, H. Park, B. Kim, J. S. Kim, K. Kang, *Trend* **2019**, *1*, 349–360; c) W. Zhao, X. Mu, P. He, H. Zhou, *Batteries* **2019**, *2*, 803–819; d) R. A. Wong, C. Yang, A. Dutta, M. O M. Hong, M. L. Thomas, K. Yamanaka, T. Ohta, K. Waki, H. R. Byon, *ACS Energy Lett.* **2018**, *3*, 592–597; e) W.-J. Kwak, J. Park, H. Kim, J. M. Joo, D. Aurbach, H. R. Byon, Y.-K. Sun, *ACS Energy Lett.* **2020**, *5*, 2122–2129.
[5] a) J. Wandt, P. Jakes, J. Granwehr, H. A. Gasteiger, R.-A. Eichel, *Angew. Chem. Int. Ed.* **2016**, *55*, 6892–6895; *Angew. Chem.* **2016**, *128*, 7006–7009; b) N. Mahne, B. Schafzahl, C. Leypold, M. Leypold, S. Grumm, A. Leitgeb, G. A. Strohmeier, M. Wilkening, O. Fontaine, D. Kramer, C. Slugovc, S. M. Borisov, S. A. Freunberger, *Nat. Energy* **2017**, *2*, 17036.
[6] a) A. T. S. Freiberg, M. K. Roos, J. Wandt, R. de Vivie-Riedle, H. A. Gasteiger, *J. Phys. Chem. A* **2018**, *122*, 8828–8839; b) J. Wandt, A. T. S. Freiberg, A. Ogrodnik, H. A. Gasteiger, *Mater. Today* **2018**, *21*, 825–833.
[7] a) M. Carboni, A. G. Marrani, R. Spezia, S. Brutti, *J. Electrochem. Soc.* **2018**, *165*, A118-A125; b) Z. Huang, H. Zeng, M. Xie, X. Lin, Z. Huang, Y. Shen, Y. Huang, *Angew. Chem. Int. Ed.* **2019**, *58*, 2345–2349; c) S. Feng, M. Huang, J. R. Lamb, W. Zhang, R. Tatara, Y. Zhang, Y. Guang Zhu, C. F. Perkinson, J. A. Johnson, Y. Shao-Horn, *Chem* **2019**, *5*, 2630–2641.
[8] K. Chaisiwamongkhol, C. Batchelor-McAuley, R. G. Palgrave, R. G. Compton, *Angew. Chem. Int. Ed.* **2018**, *57*, 6270–6273; *Angew. Chem.* **2018**, *130*, 6378–6381.
[9] W.-J. Kwak, H. Kim, Y. K. Petit, C. Leypold, T. T. Nguyen, N. Mahne, P. Redfern, L. A. Curtiss, H.-G. Jung, S. M. Borisov, S. A. Freunberger, Y.-K. Sun, *Nat. Commun.* **2019**, *10*, 1380.
[10] a) N. B. Aetukuri, B. D. McCloskey, J. M. García, L. E. Krupp, V. Viswanathan, A. C. Luntz, *Nat. Chem.* **2015**, *7*, 50–56; b) T. Liu, J. P. Vivek, E. W. Zhao, J. Lei, N. Garcia-Araez, C. P. Grey, *Chem. Rev.* **2020**, *120*, 6558–6625; c) A. Halder, H.-H. Wang, K. C. Lau, R. S. Assary, J. Lu, S. Vajda, K. Amine, L. A. Curtiss, *ACS Energy Lett.* **2018**, *3*, 1105–1109; d) T. A. Galloway, G. Attard, L. J. Hardwick, *Electrochem. Commun.* **2020**, *119*, 106814.
[11] a) M. Hong, C. Yang, R. A. Wong, A. Nakao, H. C. Choi, H. R. Byon, *J. Am. Chem. Soc.* **2018**, *140*, 6190–6193; b) Y. Wang, N.-C. Lai, Y.-R. Lu, Y. Zhou, C.-L. Dong, Y.-C. Lu, *Joule* **2018**, *2*, 2364–2380; c) Y. Wang, Y.-R. Lu, C.-L. Dong, Y.-C. Lu, *ACS Energy Lett.* **2020**, *5*, 1355–1363; d) S. Kang, Y. Mo, S. P. Ong, G. Ceder, *Chem. Mater.* **2013**, *25*, 3328–3336; e) Y.-C. Lu, Y. Shao-Horn, *J. Phys. Chem. Lett.* **2013**, *4*, 93–99; f) Y. Mo, S. P. Ong, G. Ceder, *Phys. Rev. B* **2011**, *84*, 205446; g) Y.-C. Lu, B. M. Gallant, D. G. Kwabi, J. R. Harding, R. R. Mitchell, M. S. Whittingham, Y. Shao-Horn, *Energy Environ. Sci.* **2013**, *6*, 750–768; h) S. Ganapathy, B. D. Adams, G. Stenou, M. S. Anastasaki, K. Goubitz, X.-F. Miao, L. F. Nazar, M. Wagemaker, *J. Am. Chem. Soc.* **2014**, *136*, 16335–16344.
[12] W. H. Koppenol, *Nature* **1976**, *262*, 420–421.
[13] a) N. Mahne, S. E. Renfrew, B. D. McCloskey, S. A. Freunberger, *Angew. Chem. Int. Ed.* **2018**, *57*, 5529–5533; b) G. Houchins, V. Pande, V. Viswanathan, *ACS Energy Lett.* **2020**, *5*, 1893–1899.
[14] E. Mourad, Y. K. Petit, R. Spezia, A. Samojlov, F. F. Summa, C. Prehal, C. Leypold, N. Mahne, C. Slugovc, O. Fontaine, S. Brutti, S. A. Freunberger, *Energy Environ. Sci.* **2019**, *12*, 2559–2568.
[15] L. Qin, L. Schkeryantz, J. Zheng, N. Xiao, Y. Wu, *J. Am. Chem. Soc.* **2020**, *142*, 11629–11640.
[16] a) V. S. Bryantsev, M. Blanco, F. Faglioni, *J. Phys. Chem. A* **2010**, *114*, 8165–8169; b) U. Das, K. C. Lau, P. C. Redfern, L. A. Curtiss, *J. Phys. Chem. Lett.* **2014**, *5*, 813–819.
[17] a) A. U. Khan, *J. Am. Chem. Soc.* **1981**, *103*, 6516–6517; b) E. J. Corey, M. M. Mehrotra, A. U. Khan, *Biochem. Biophys. Res. Commun.* **1987**, *145*, 842–846; c) E. A. Mayeda, A. J. Bard, *J. Am. Chem. Soc.* **1974**, *96*, 4023–4024.
[18] D. H. Chin, G. Chiericato, E. J. Nanni, D. T. Sawyer, *J. Am. Chem. Soc.* **1982**, *104*, 1296–1299.
[19] a) J. M. Aubry, J. Rigaudy, C. Ferradini, J. Pucheault, *J. Am. Chem. Soc.* **1981**, *103*, 4965–4966; b) E. J. Nanni, R. R. Birge, L. M. Hubbard, M. M. Morrison, D. T. Sawyer, *Inorg. Chem.* **1981**, *20*, 737–741.
[20] A. Pierini, S. Brutti, E. Bodo, *ChemPhysChem* **2020**, *21*, 2060–2067.
[21] a) L. Schafzahl, N. Mahne, B. Schafzahl, M. Wilkening, C. Slugovc, S. M. Borisov, S. A. Freunberger, *Angew. Chem. Int. Ed.* **2017**, *56*, 15728–15732; b) I. Lozano, D. Córdoba, H. B. Rodríguez, I. Landa-Medrano, N. Ortiz-Vitoriano, T. Rojo, I. R. de Larramendi, E. J. Calvo, *J. Electroanal. Chem.* **2020**, *872*, 114265.
[22] A. Samojlov, D. Schuster, J. Kahr, S. A. Freunberger, *Electrochim. Acta* **2020**, *362*, 137175.
[23] a) A. Faucitano, A. Buttafava, F. Martinotti, P. Bortolus, *J. Phys. Chem.* **1984**, *88*, 1187–1190; b) G. Nardi, I. Manet, S. Monti, M. A. Miranda, V. Lhiaubet-Vallet, *Free Radical Biol. Med.* **2014**, *77*, 64–70.
[24] Y. K. Petit, C. Leypold, N. Mahne, E. Mourad, L. Schafzahl, C. Slugovc, S. M. Borisov, S. A. Freunberger, *Angew. Chem. Int. Ed.* **2019**, *58*, 6535–6539.
[25] A. Tkacheva, J. Zhang, B. Sun, D. Zhou, G. Wang, A. M. McDonagh, *J. Phys. Chem. C* **2020**, *124*, 5087–5092.
[26] D. Córdoba, H. B. Rodríguez, E. J. Calvo, *ChemistrySelect* **2019**, *4*, 12304–12307.
[27] a) C. Schweitzer, R. Schmidt, *Chem. Rev.* **2003**, *103*, 1685–1758; b) C. S. Foote, E. L. Clennan, C. S. Foote, J. S. Valentine, A. Greenberg, J. F. Liebman, *Active Oxygen in Chemistry*, Springer Netherlands, Dordrecht, **1995**, pp. 105–140.
[28] a) J. R. Harbour, S. L. Issler, *J. Am. Chem. Soc.* **1982**, *104*, 903–905; b) W. R. Haag, T. Mill, *Photochem. Photobiol.* **1987**, *45*, 317–321.
[29] A. Maldotti, R. Amadelli, V. Carassiti, *Can. J. Chem.* **1988**, *66*, 76–80.
[30] a) C. Schweitzer, Z. Mehrdad, F. Shafii, R. Schmidt, *J. Phys. Chem. A* **2001**, *105*, 5309–5316; b) C. Schweitzer, Z. Mehrdad, F. Shafii, R. Schmidt, *Phys. Chem. Chem. Phys.* **2001**, *3*, 3095–3101.
[31] W.-J. Kwak, S. A. Freunberger, H. Kim, J. Park, T. T. Nguyen, H.-G. Jung, H. R. Byon, Y.-K. Sun, *ACS Catal.* **2019**, *9*, 9914–9922.
[32] Z. Liang, Q. Zou, J. Xie, Y.-C. Lu, *Energy Environ. Sci.* **2020**, *13*, 2870–2877.

Manuscript received: September 8, 2020
Revised manuscript received: October 26, 2020
Accepted manuscript online: November 17, 2020
Version of record online: December 1, 2020